ON THE DYNAMIC OF SONIC COMPOSITES

NICOLETA STAN , LIGIA MUNTEANU, VETURIA CHIROIU,
VALERICA MOSNEGUTU, MARIUS IONESCU

Abstract. The paper is concerned with the full band-gaps size and the localized modes around interfaces in a multilayer film. The film consists of alternating layers of piezoelectric ceramics and epoxy resin following a triadic Cantor sequence. The Cantor structure is characterized by anharmonic coupling between the extended-mode (phonon) and the localized-mode (fracton) vibration regimes, and by extremely low thresholds for subharmonic generation of ultrasonic waves, as compared to the corresponding homogeneous and periodical ones. The dynamic optimization tracks the enhancing of full band-gaps for both Lamb and Love waves.

Key words: vibration, full band-gaps, Cantor sequence.

1. INTRODUCTION

There is a broad class of structures (aperiodic crystals) which exhibit long-range order without lattice translation symmetry [1]. A crystal structure exhibits periodicity in 3D generated by translational symmetry which produce additional sharp Bragg reflections that cannot be described in terms of only three *hkl* indices. When the description of the structure is extended to four or more dimensions, it can be seen that the structure is indeed periodic in higher-dimensional spaces. This is the basis of superspace crystallography used to describe the aperiodic crystals.

The term 'modulation' reflects the variation of the atomic positions concerning an ideal periodic structure. It derives from the atomic modulation wavefunctions in the description of these structures. When the wavelength is incommensurate with the average periodic lattice, it disrupts the long-range periodicity. A modulated structure is more than a structure derived from treatment of the variances in atomic positions and occupancies. It can reveal the causes of the atomic displacements and provide insights to the properties (magnetic, superconducting etc.) of these structures possess.

The study of modulated structures is an active field in crystallography.

The metallic bilayers as Au/Ni, Cu/Pd, etc., represent a class of films that contain 1D short-wavelength modulation given by the vapor deposition. The waves

Institute of Solid Mechanics, Romanian Academy

Ro. J. Techn. Sci. – Appl. Mechanics, Vol. 69, N^{os} 2–3, P. 127–138, Bucharest, 2024

DOI:10.59277/RJTS-AM.2024.2-3.02

have an orientation of [111] normal to the plane of the film. Experimentally, it was shown the increase of the elastic modulus in metallic multilayer structures as Au-Ni, Cu-Pd, Cu-Ni, Ag-Pd [2–5].

It was observed that the measured biaxial modulus was two to three times larger than the value predicted by the simple rule of mixture for a distance in the range of 15–20 microns [2]. A Cu-Ni foil of 66% Cu has a Young modulus Y[100] of 0.23 TPa which is over 50% greater than that of a Cu-Ni alloy of the same copper composition for which Y[100] = 0.14 TPa [3].

The enhancement of the Young modulus for a material is known in the literature as the supermodulus effect [4, 5]. The origin of the supermodulus effect can be found on the micro-scale where the larger lattice constant is compressed laterally whereas the component with the smaller lattice constant is expanded. The coherence strains in the interface minimise the total energy of the material by adjusting the interlayer spacing perpendicular to the plane of the interface. In the [100] direction, the distribution of strain in the structure is represented in Fig. 1.

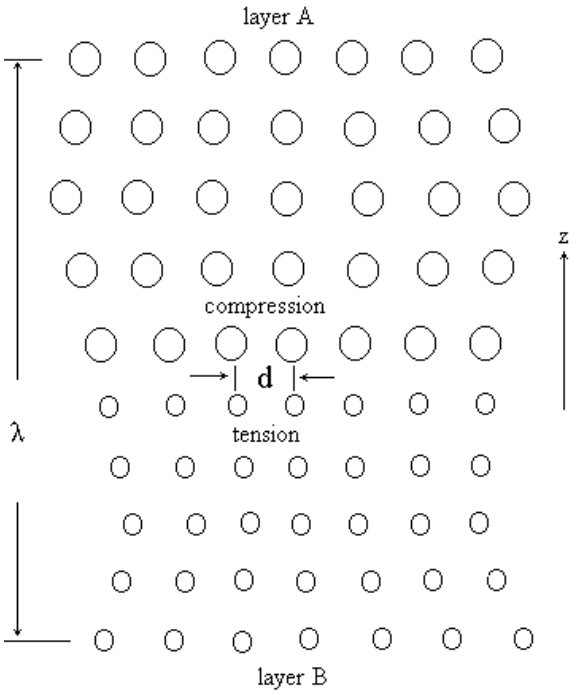

Fig. 1 – A multilayer interface subjected to compression and tension.

The beam considered in this paper has the length L, the width of the smallest layer $L/81$ and the thickness h. The distance between two atoms of layer A and respectivelly B, is d.

To determine the displacement field $u(x,t)$, $x=(x_1,x_2,x_3)$ and the Cauchy stress distribution σ_{ij}, $i,j=1,2,3$, as functions of position in the reference configuration and time, the reference coordinate system $Ox_1x_2x_3$ is introduced, with origin at the left end of the beam, in the middle plane of the beam with the axis Ox_1 in plane and normal to the layers and Ox_3 out of plane, normal to the beam. The index 1 refers to material A and index 2 to the material B.

The beam is characterized by the mass density ρ_1 and ρ_2, the specific internal energy E_i and E_2 and the stress response functions σ_{ij}^1 and σ_{ij}^2, $i,j=1,2,3$, respectively .

The deformation of the beam is expressed by the deformation gradient

$$F_{ij}=\delta_{ij}+\frac{\partial u_1}{\partial x_j}. \tag{1}$$

The right and left Cauchy-Green deformation tensors are

$$C_{ij}=F_{ki}F_{kj}, \quad B_{ij}=F_{ik}F_{jk}, \tag{2}$$

and the Lagrange strain tensor

$$E_{ij}=\frac{1}{2}\left(F_{ki}F_{kj}-\delta_{ij}\right). \tag{3}$$

The invariant of B is written as

$$I_1=\mathrm{tr}(B)=B_{kk}, \tag{4}$$

and the force per unit deformed area (Cauchy stress) is

$$n_i\sigma_{ij}=\lim_{dA\to 0}\frac{\mathrm{d}P_j^{(n)}}{\mathrm{d}A}. \tag{5}$$

The constitutive laws for elastic materials are

$$\sigma_{ij}-\frac{1}{J}F_{ik}\frac{\partial W}{\partial F_{jk}}, \tag{6}$$

where W is the Helmholtz free energy.

The materials exhibit fluctuations of atomic distance as shown in Fig. 2a. An example of a general atomic structure can be presented in Fig. 2b, where 1, 2, and 3 show different atoms [3, 5].

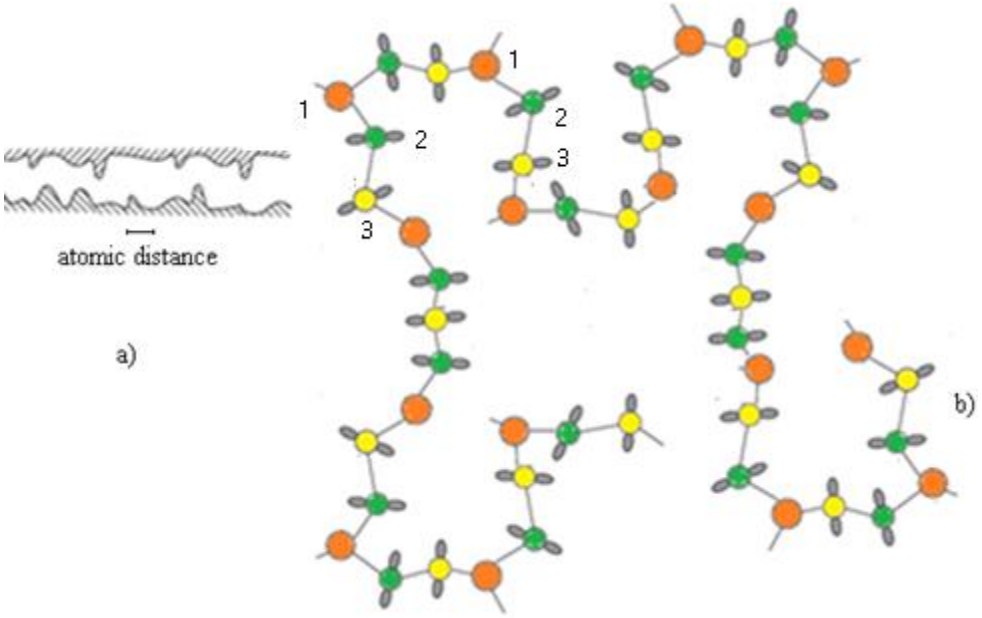

Fig. 2 – a) Fluctuations of the atomic distances; b) example of the atomic structure of the material.

The fluctuations appear to be the small length of action forces from the amorphous material. The response of materials to external forces within a length and time scale that exceeds the domain of applicability of a classical theory depends on the ratio $(\lambda / l, \tau / \tau_0)$ or $(\lambda / l, \omega_0 / \omega)$, where λ is a characteristic length of the glass (atomic distance, granular distance, etc.), l is the external characteristic length associated with the external forces (waves, distances over which load distribution change sharply, geometrical and surface discontinuities), τ the time scale (or frequency ω) which is the transmission time of a signal (or a frequency), and τ_0 is the external characteristic time or frequency) associated with the external forces [4, 5].

For $\lambda / l << 1$ and $\tau / \tau_0 << 1$, the external forces excite large numbers of subbodies simultaneously, so that subbodies interact and the result is a statistical average of the individual responses. For $\lambda / l = 1$ and $\tau / \tau_0 = 1$, individual fields of subbodies (intermolecular and atomic forces) are important.

The problem we consider now is to optimize the full band-gap interval of frequencies in which waves cannot propagate in the thin film. The unknown quantoties are thickness h, the depth d and the order n of the Cantor sequence. The uncertain parameters are related to the boundary conditions on the interfaces

between constituents where the displacement and the traction vectors can be discontinuous.

Maximizing the full band-gaps is taken as the objective, while structural integrity is taken as the constraint. Then the optimum design is carried out under interval uncertainty

$$[u_1]=[u_3]=\Delta_1\in[-a,a],\quad [t_{11}]=[t_{13}]=\Delta_2\in[-b,b], \tag{7}$$

with a,b real numbers.

The Cantor sequence {\displaystyle {\mathcal {C}}} is a process created by deleting the open middle third from a line. This process can be infinit. We delete the open middle third (1/3, 2/3) from the interval [0, 1] and leave two line segments $[0,\ 1/3]\cup[2/3,\ 1]$. Next, the open middle third of each of these remaining segments is deleted, leaving four line segments $[0,\ 1/9]\cup[2/9,\ 1/3]\cup[2/3,\ 7/9]\cup[8/9,\ 1]$. The n^{th} set for $n\geq 1$ is $C_n=\dfrac{C_{n-1}}{3}\cup\left(\dfrac{2}{3}+\dfrac{C_{n-1}}{3}\right)$, $C_0=[0,1]$, with the geometric progression $\sum_{n=0}^{\infty}\dfrac{2^n}{3^{n+1}}=1$.

The standard procedure for analyzing the problem (1)–(7) is to seek eigenfunctions in the form of Bloch modes, and then the generation of local band-gaps. The band-gaps are generated in the band structure of the film, meaning that the waves are forbidden to propagate with certain frequencies in Ox_1 direction. Alongside of Lamb waves there is another kind of motion of particles,namely in-plane but in a direction perpendicular to the direction of wave propagation. These are Love waves (SH waves). We are interested to optimize the full band-gaps so that to cover both waves the Lamb and the Love waves that are propagating in the Ox_1 direction. The full band-gap depends on the thickness and grain size of the thin film. The grain size mainly depends on the film thickness. So, if the composition changed with thickness, it will directly affect the thin film band gap. Lastly, the grain size of the thin film afect the average transmission of the film, due to the scattering, but not affecting the energy band gap until the composition is not varying.

The calculus is carried out for $l=68$ mm, $a=b=10$. The resonant Lamb modes are excited by applying an external electric field $\bar{E}_1=\bar{E}_3=\bar{E}^0\exp(\mathrm{i}\omega_0 t)$ on both sides of the plate. The surface Lamb waves are superposition of longitudinal (symmetric waves) and shear modes (anti-symmetric waves or SV waves), which dominate the radial in-plane and vertical motion of particles in the film.

The material constants for piezoelectric ceramics and epoxy resin are shown in Table 1. The structure and size of the band-gap depend on $\bar{E}^0$. If $\bar{E}^0$ is increased above a threshold value $\bar{E}^0_{th} = 5.27\,\mathrm{V}$, the $\omega/2$ subharmonic generation is observed. The result of superposition of normal and subharmonic modes is the generation of two kind of vibration regimes: a localised-mode (fracton) regime and an extended-vibration (phonon) regime.

Table 1

The material constants for piezoelectric ceramics and epoxy resin

	λ GPa	μ GPa	A GPa	B GPa	C GPa	$\bar{\varepsilon}$ nF/m	$\bar{\varepsilon}_1$ nF/m	e_1 nm/V	$\bar{e}_1 = \bar{\bar{e}}_1$ nm/V	ρ kg/m^3
piezo-electric	71.6	35.8	− 2000	− 1134	− 900	4.065	2.079	− 0.218	− 0.435	7650
epoxy resin	42.31	3.76	2.8	9.7	− 5.7	-	-	-	-	1170

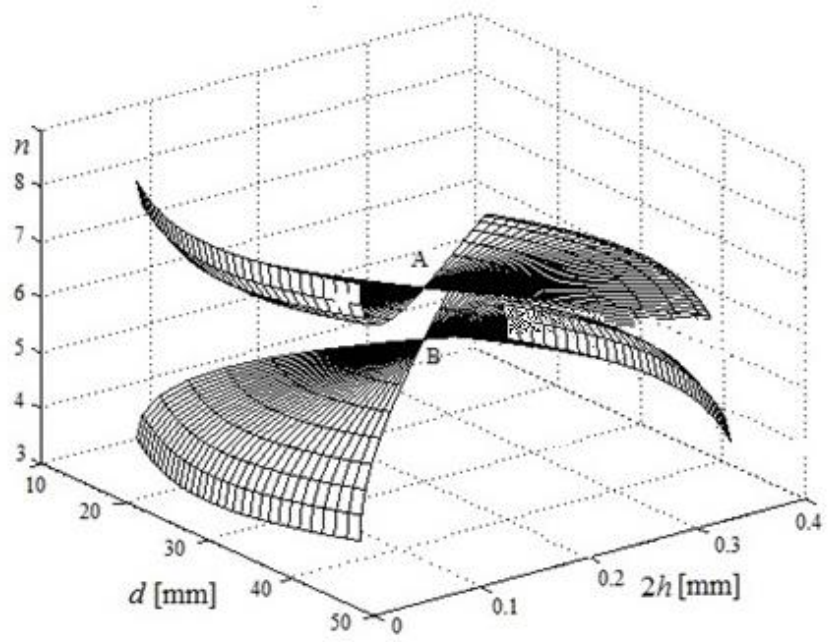

Fig. 3 – Two solutions of the genetic algorithm.

The fracton vibrations are mostly localized on a few elements, while the phonon vibrations essentially extend to the whole plate. For the homogeneous plate

the mismatch $\omega_n - \omega/2$ is due to the symmetry of fundamental modes with piezoelectric ceramics and epoxy resin mode. Fig. 3 shows two solutions of the genetic algorithm, named A and B. The solution A is removed because it leads to the values that are outside the allowed area of the computed eigenfrequencies given by Table 2.

Table 2

Computed eigenfrequencies

$\omega/2\pi$ [Hz] $n=3$	100.2 $\pm$0.05	167 $\pm$ 0.01	200.4 $\pm$0.03	250.5 $\pm$0.1	334 $\pm$0.1	367.4 $\pm$0.05	400.8 $\pm$0.1	501 $\pm$0.02	584.5 $\pm$0.1
$\omega/2\pi$ [Hz] $n=4$	132.4 $\pm$ 0.01	171.3 $\pm$0.03	231.9 $\pm$0.04	264.8 $\pm$0.1	342.6 $\pm$0.1	409 $\pm$0.03	463.8 $\pm$0.02	524.9 $\pm$0.04	685.2 $\pm$0.1

Figure 4 shows the full band-gap including both Lamb and Love waves, for $n=3$ and $n=4$, respectively. We draw from this figure the conclusion that the size of the band-gap is favoured for $n=4$.

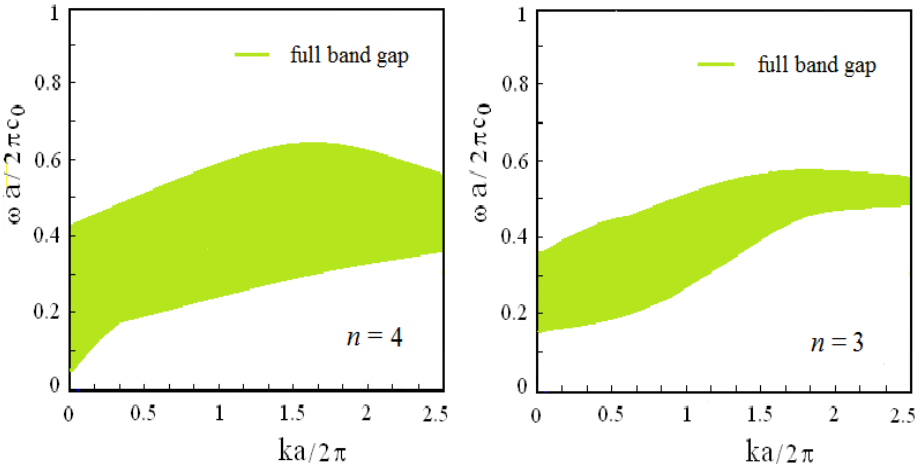

Fig. 4 – The full band-gaps for n = 3 and n = 4.

The Cantor structure is characterized by anharmonic coupling between the extended-mode (phonon) and the localized-mode (the fracton) vibration regimes, and by extremely low thresholds for subharmonic generation of ultrasonic waves, as compared to the corresponding homogeneous and periodical ones [13–14].

The fracton and phonon regimes are represented in Figs. 4 and 5, for n = 3 and $\omega/2\pi = 167$ Hz, and n = 4 and $\omega/2\pi = 171.3$ Hz, respectively.

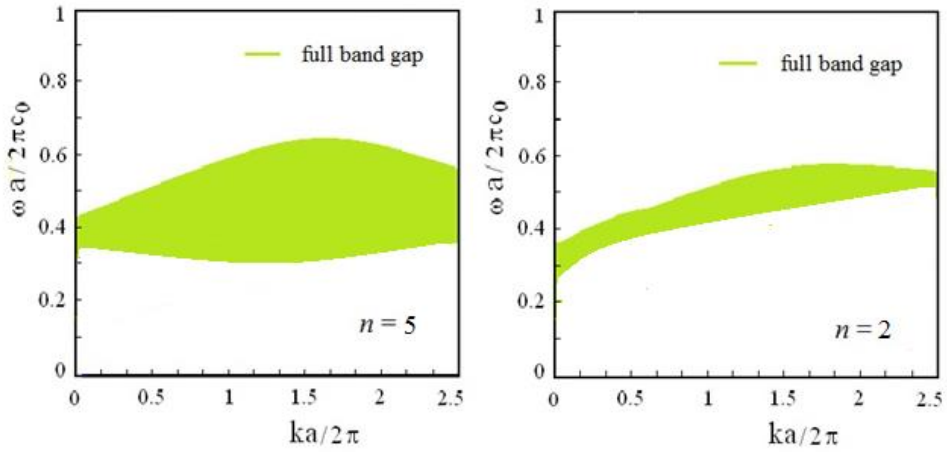

Fig. 5 – The full band-gaps for $n = 5$ and $n = 2$.

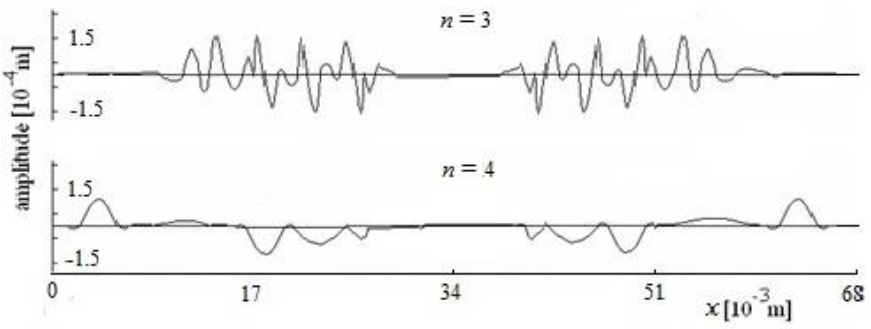

Fig. 6 – The fracton regime for $n = 3$ and $n = 4$.

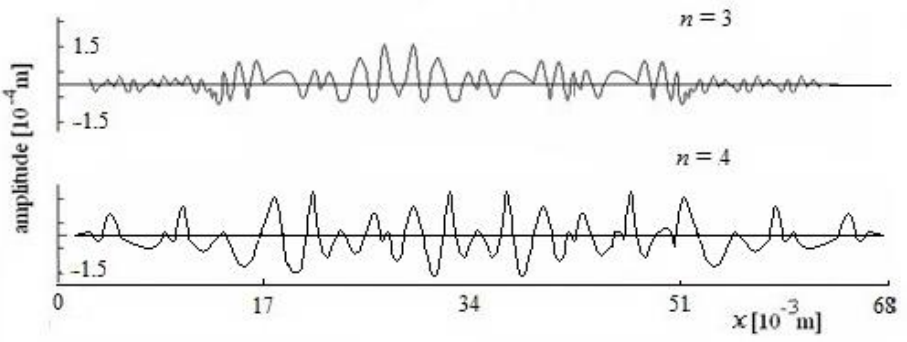

Fig. 7 – The phonon regime for $n = 3$ and $n = 4$.

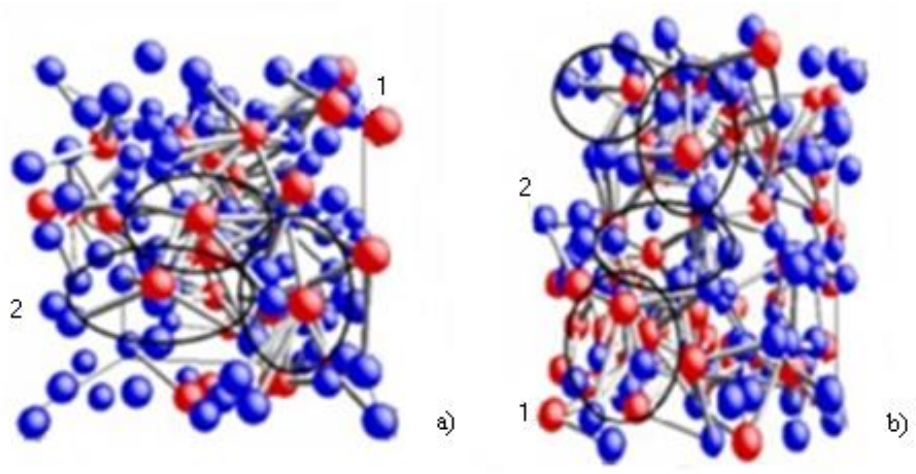

Fig. 8 – a) The distribution of atoms; b) 3D bonds.

Figure 6 represents the fracton regime for n = 3 and n = 4. In Fig. 7 is presented the phonon regime for n = 3 and n = 4 and in Fig. 8 the distribution of atoms (a) and 3D bonds (b) are done. Figure 9 presents the amplitudes of the surface displacement for 310 nm and the subharmonic 155 nm.

The amplitudes of the surface displacement for 620 nm and the subharmonic 315 nm are presented in Fig.10. Amplitudes of the surface displacement for 802 nm and the subharmonic 401 nm are presented in Fig. 11, while Fig. 12 and Fig. 13 show the amplitudes of the surface displacement for localized vibration modes at 1 200, 1 600 and 1 900 nm, and respectively the amplitudes of the surface displacement for extended vibration modes for 1 360 nm and 1 460 nm.

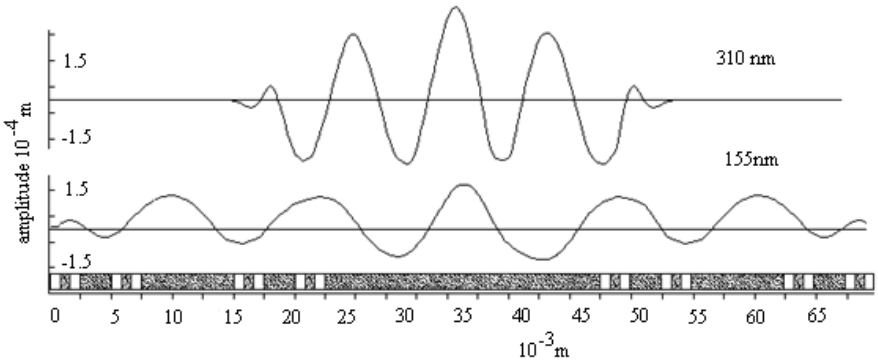

Fig. 9 – Amplitudes of the surface displacement for 310 nm and the subharmonic 155 nm.

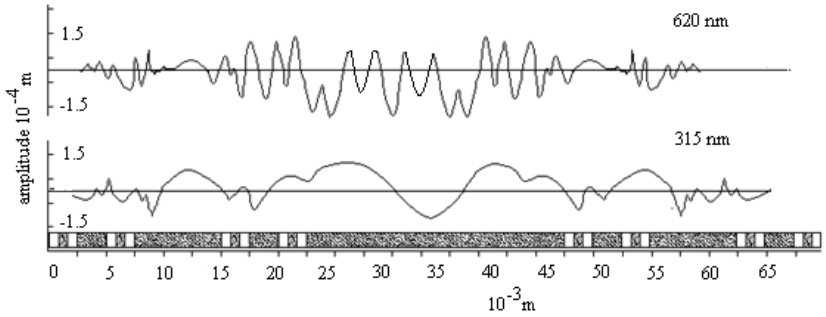

Fig. 10 – Amplitudes of the surface displacement for 620 nm and the subharmonic 315 nm.

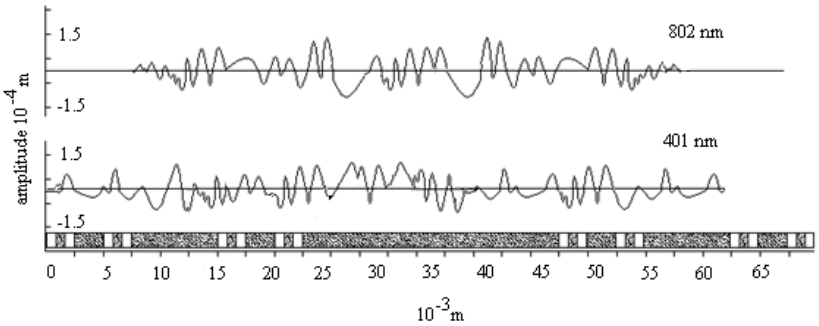

Fig. 11 – Amplitudes of the surface displacement for 802 nm and the subharmonic 401 nm.

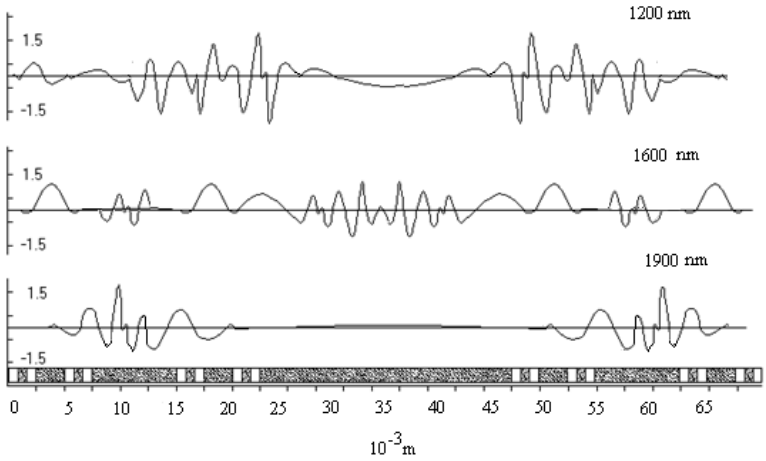

Fig. 12 – The amplitudes of the surface displacement for localised vibration modes at 1200, 1600 and 1900 nm.

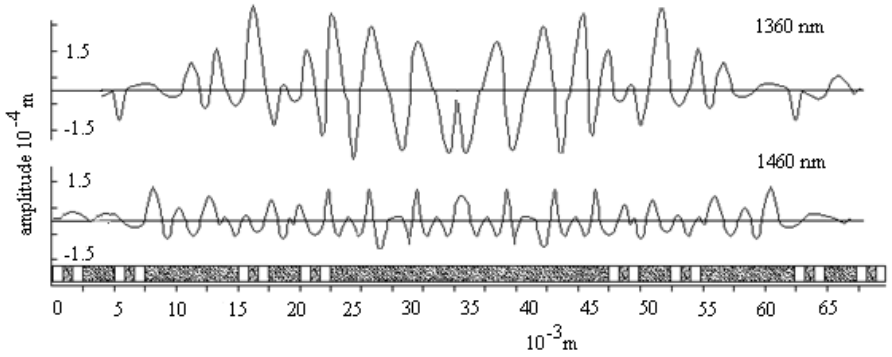

Fig. 13 – The amplitudes of the surface displacement for extended vibration modes for 1360 nm and 1460 nm.

2. CONCLUSIONS

Two kinds of vibrations are found: a localized mode or the fracton regime and an extended vibration or the phonon regime. The fraction vibrations are localized on a few elements of the plate, while the phonon vibrations extend to the whole chalcogenide plate. In the case of a periodical plate the dispersion prevents the matching of frequencies of the fundamental and appropriate subharmonic vibration modes. For the homogeneous beam the mismatch interval is due to the symmetry of fundamental vibration modes. Only symmetric odd n can induce a subharmonic, but the normal amplitude never coincides with a plate vibration mode. For the chalcogenide Cantor plate, we have obtained the same qualitative results as Craciun and Alippi. Given a normal vibration mode, the value of the expected threshold which describe the ability of generating subharmonics, is determined by the existence of a normal mode with small frequency mismatch between their amplitudes and large spatial overlap between the fundamental and subharmonic displacement field.

Received on June, 2024

REFERENCES

1. JANKOWSKI, A.F., TSAKALAKOS, T., *The effect of strain on the elastic constants of noble metals*, J. Phys. F: Met. Phys., **15**, pp. 1279–1292, 1985.
2. YANG, W. M. C., TSAKALAKOS, T., HILLIARD, J. E., *Enhanced elastic modulus in composition-modulated gold-nickel and copper-palladium foils*, J. Appl. Phys., **48**, pp. 876–879, 1977.

3. TSAKALAKOS, T., HILLIARD, J. E., *Elastic modulus in composition-modulated copper-nickel foils*, J. Appl. Phys., **54**, *2*, pp. 734–737, 1983.
4. JANKOWSKI, A. F., *Modelling the supermodulus effect in metallic multilayers*, J. Phys. F: Met. Phys., **18**, pp. 413–427, 1988.
5. DELSANTO, P.P., PROVENZANO, V., UBERALL, H., *Coherency strain effects in metalic bilayers*, J. Phys.: Condens. Matter, **4**, pp. 3915–3928, 1992.
6. THOMAS, J. F. JR., *Pseudopotential calculation of the third-order elastic constants of copper and silver*, Phys. Rev. B, **7**, *6*, pp. 2385–2392, 1973.
7. GREEN, A. E., ZERNA, W., *Theoretical Elasticity*, Oxford Univ. Press, New York, 1963.
8. ACHENBACH, J. D., *Wave Propagation in Elastic Solids*, Nort-Holland Publ. Co., 1976.
9. TRUESDELL, C., NOLL, W., *The non-linear field theories of mechanics*, in Handbuch der Physik, ed. S. Flugge, III, 3, 1965.
10. TEODOSIU, C., *Elastic models of crystal defects*, Edit. Academiei, Springer-Verlag, 1982.
11. CHIROIU, V. CHIROIU, C., *Inverse problems in mechanics* (in Romanian), Edit. Academiei, Bucharest, 2003.
12. CHIROIU, V. BRISAN, C. GIRIP, I., *On the dynamic optimisation of sonic composites*, Romanian Journal of Mechanics, **1**, *1*, pp. 3–12, 2016.
13. GILBERT, R., HACKL, K., XU, Y., *Inverse problem for wave propagation in a perturbed layered half-space*, Mathematical and Computer Modelling, **45**, pp. 21–33, 2007.
14. LERNER, R.M., PARKER, K.J., HOLEN, J., GRAMIAK, R., WAAG, R.C., *Sonoelasticity: Medical Elasticity Images Derived from Ultrasound Signals in Mechanically Vibrated Targets*, Acoustical Imaging, **16**, pp. 317–327, 1988.